Proceedings of the Thirty-fifth (2025) International Ocean and Polar Engineering Conference **www.isope.org**
Seoul/Goyang, Korea, June 1-6, 2025
Copyright © 2025 by the International Society of Offshore and Polar Engineers (ISOPE)
ISBN 978-1-880653-74-6; ISSN 1098-6189

Aerodynamic Performance of NREL 5MW Wind Turbine under Forced Surge Motion Considering Blade Elasticity

Min Li[1], *Jinguang Wang*[2], *Weiwen Zhao*[1], *Decheng Wan*[1*]

[1] Computational Marine Hydrodynamics Lab (CMHL), School of Naval Architecture, Ocean and Civil Engineering, Shanghai Jiao Tong University, Shanghai, China
[2] Zhongnan Engineering Corporation Limited, Changsha, China

[*]Corresponding Author

ABSTRACT

To precisely understand the independent impacts and interaction mechanisms of various motion factors on the aerodynamic response of wind turbines, this study employs computational fluid dynamics (CFD) methods, utilizing the FEWT-SJTU solver, to examine the effects of forced surge motion on wind turbines' dynamic behavior. The study finds that increasing forced motion amplitude leads to nearly linear rises in power and thrust fluctuations, spreading attack angles, and more pronounced blade deformations, while period changes cause only slight decreases in mean power and thrust with more moderate fluctuations. This research offers valuable insights for optimizing turbine design and operation, highlighting that amplitude has a more significant impact on turbine performance and deformation than period.

KEY WORDS: Floating wind turbine; forced surge motion; aero-elastic; FEWT-SJTU.

INTRODUCTION

As modern society advances at a rapid pace, the transition to renewable energy sources, particularly wind power, is gaining momentum as a substitute for fossil fuels. However, the complex marine environment, characterized by wind, waves, and currents, causes motion in offshore platforms. This motion can lead to fluctuations in the power output of wind turbines, which can directly affect the turbine's stability and operational efficiency. Moreover, the platform's response to motion is further complicated by blade deformation and variations in aerodynamic performance. Decoupling these perturbations is essential for understanding and optimizing the design and operation of floating wind turbines. Only through a detailed analysis and quantitative description of these interactions can we develop effective strategies to ensure the reliability and economic viability of floating wind turbines in challenging marine conditions.

The primary research methods for investigating the aerodynamic performance of wind turbines encompass wind tunnel tests (Fang et al., 2020; Fontanella et al., 2022; Meng et al., 2022) and numerical simulations. To ensure the controllability and repeatability of experimental procedures, as well as the computational efficiency of numerical analyses, previous studies have delved into the impact of specified platform motions on the unsteady aerodynamic responses of floating wind turbines. Concurrently, by prescribing particular platform motions, these studies have been able to isolate the effects of individual motions or specific combinations thereof on the aerodynamic response of the turbines. This approach facilitates a more precise understanding of the independent impacts and interaction mechanisms of various motion factors.

Currently, numerous scholars are employing Computational Fluid Dynamics (CFD) methods to investigate the impact of platform motion on the unsteady aerodynamic performance of wind turbines (Feng et al., 2021; Chen et al., 2022). CFD techniques offer highly accurate aerodynamic performance calculations, capable of simulating complex aerodynamic phenomena and providing comprehensive flow field information. They also allow for the substitution of real wind turbine blades with actuator lines, thereby avoiding the need to solve the boundary layer on the blade surface. This approach effectively reduces computational resource demands while maintaining high accuracy. Fang et al. (2021) utilized CFD to examine the aerodynamic performance and wake characteristics of a floating horizontal-axis wind turbine under longitudinal motion at a 1:50 model scale. They discovered that even a small amplitude of longitudinal motion significantly affects the rotor's thrust, torque, and power, as well as altering the near and far wake characteristics. Alkhabbaz et al. (2024) conducted high-fidelity CFD simulations to study the effect of the longitudinal motion of a semi-submersible platform on the aerodynamic performance and wake characteristics of an NREL 5-MW floating wind turbine. Their findings indicated that longitudinal motion substantially influences the apparent wind speed perpendicular to the rotor plane, leading to power output fluctuations over the longitudinal cycle and a faster wake recovery compared to a stationary wind turbine. Wang et al.

(2024) used CFD methods to investigate the aerodynamic performance of a floating wind turbine under coupled blade rotational and translational motions. They analyzed the effects of different translational frequencies and amplitudes on aerodynamic loads, blade pressure distributions, and wake characteristics. Cheng et al. (2019) analyzed the unsteady aerodynamic performance of an NREL 5 MW wind turbine under periodic longitudinal oscillation and longitudinal rocking motions using the OpenFOAM open-source software. They explored the influence of platform motion amplitude on the aerodynamic loads of the wind turbine and analyzed the tower shadow effect. Cai et al. (2024) applied the CFD method to model the wind turbine and investigate its aerodynamic performance under longitudinal oscillation, as well as the coupling conditions of longitudinal oscillation and other motions. They revealed significant changes in the aerodynamic characteristics of the wind turbine under these conditions. While domestic and international scholars have conducted extensive research using the aforementioned methods, fewer studies have focused on the effects of forced surge motion considering blade deformation.

In this paper, based on the FEWT-SJTU solver from the CMHL of Shanghai Jiao Tong University, we perform detailed calculations to assess the aerodynamic performance and blade deformation of the NREL 5MW wind turbine under forced surge motion. Our research specifically targets the unsteady aerodynamic response and blade deformation of the wind turbine under varying parameters of surge motion, all within the context of uniform wind conditions. The paper provides a comprehensive introduction to the structural calculation method, the prediction method for aerodynamic performance, and the coupling strategy employed. We also meticulously describe the calculation conditions and the model used, and validate the accuracy and reliability of our computational results. Ultimately, our analysis delves into the impact of different forced motion amplitudes and periods of the floating wind turbine on both its aerodynamic performance and blade deformation, offering valuable insights into the dynamic behavior of such systems under specified operational conditions.

METHODOLOGY

Structural model

In this paper, the Euler-Bernoulli beam model is employed to represent the blade equivalently for deformation calculations. The blade is discretized using the one-dimensional finite element method. The structural dynamics equation utilized to solve for the blade deformation is as follows:

$$\boldsymbol{M}\ddot{\boldsymbol{x}} + \boldsymbol{C}\dot{\boldsymbol{x}} + \boldsymbol{K}\boldsymbol{x} = \boldsymbol{f} \tag{1}$$

where, **M** is the mass matrix, **C** is the damping matrix, and **K** is the stiffness matrix, while $\boldsymbol{x}$ represents the displacement vector. The damping uses Rayleigh damping, which is linearly superimposed by the stiffness matrix and the mass matrix.

$$\boldsymbol{C} = \alpha\boldsymbol{M} + \beta\boldsymbol{K} \tag{2}$$

The coupling between the various deformations of the blade is considered. The off-diagonal elements of the stiffness matrix represents the coupling effect between the flapwise deformation and the edgewise deformation, which is caused by the pre-twisting of the blade. The coupling between the torsional deformation and the bending deformation is caused by the non-coincidence of the shear center, the aerodynamic center and the center of gravity, and the coupling is realized by adding the equivalent torque to the external load.

Unsteady actuator line model

Compared to fixed wind turbines, floating wind turbines exhibit a more complex six-degrees-of-freedom motion, which significantly alters the flow field near the blades. At each blade section, the velocity vector of the unsteady actuator line model is the resultant of the velocity vectors caused by the platform motion, the inflow wind, and the blade rotation.

$$\boldsymbol{f} = (\boldsymbol{L}, \boldsymbol{D}) = \rho \boldsymbol{U}_{\mathrm{rel}}^2 c N_{\mathrm{b}} (C_L \boldsymbol{e}_L + C_D \boldsymbol{e}_D) \tag{3}$$

where, $\boldsymbol{L}$ and $\boldsymbol{D}$ is the lift and drag on the airfoil interface; $\boldsymbol{U}_{\mathrm{rel}}$ is the relative wind speed at the cross section of the blade, as shown in Fig. 1, $\boldsymbol{U}_{\mathrm{motion}}$ is the additional speed of the platform motion, $\boldsymbol{U}_{\mathrm{int}}$is the wind speed of the incoming flow, and $\boldsymbol{U}_{\mathrm{rot}}$ is the linear velocity of the actuator caused by the rotation of the blade ; c is the chord length of the airfoil section ; N_b is the number of blades of a single wind turbine ; $C_L$and C_D is the lift coefficient and drag coefficient ; $\boldsymbol{e}_L$and $\boldsymbol{e}_D$ is the unit vector in the x and y directions in the body coordinate.

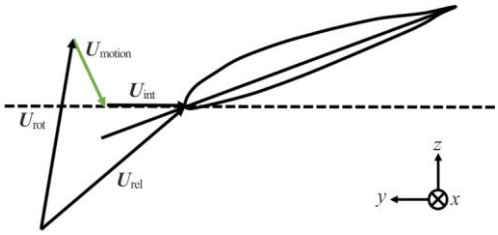

Fig. 1 Induced velocity vector diagram of the airfoil

Coupled strategy

The coupling between blade deformation and aerodynamic load is achieved by exchanging displacement and force data at the end of each time step calculation. The detailed calculation process is illustrated in Fig. 2. When computing the aerodynamic load using the unsteady actuator line model, it is essential to account for the changes in blade position and inflow wind speed due to platform motion. In this study, we simulate platform motion with a forced motion to influence the calculation of the aerodynamic load.

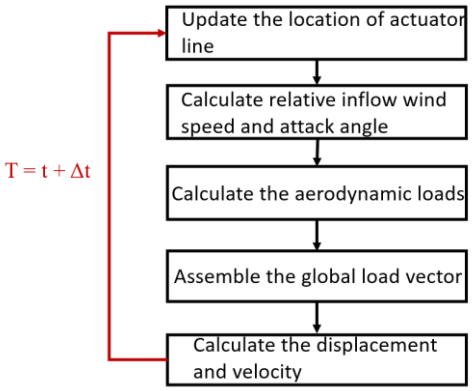

Fig. 2 Fluid-structure coupling calculation of wind turbine blades

NUMERICAL SETUP

Wind turbine

The wind turbine utilized in this study is an NREL 5MW model, featuring three blades with a rotor disc diameter of 126 meters. It has a rated wind speed of 11.4 m/s, a hub height of 189 meters, and operates at a rated rotational speed of 12.1 revolutions per minute. For a comprehensive list of additional parameters can refer to Jonkman et al. (2009).

Computational domain and mesh

The computational domain is illustrated in Fig. 3, with dimensions of 756 meters in length, 378 meters in width, and 378 meters in height. The wind turbine is situated 126 meters downstream from the inlet boundary. The top boundary and the bottom boundary is set as a slip condition, and the left and right sides are defined by symmetry boundary conditions.

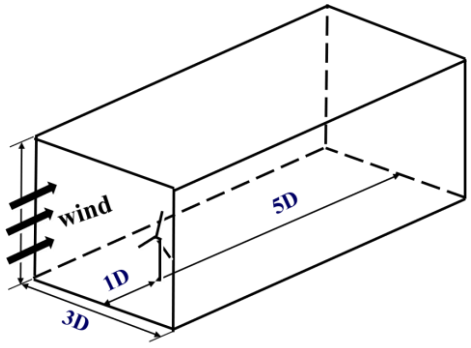

Fig. 3 Computational domain

The computational domain grid is depicted in Fig. 4, with grids uniformly distributed in the x, y, and z directions. To ensure accurate capture of flow field changes near the wind turbine and within the wake region while minimizing computational load, we initially performed grid refinement over a larger area and subsequently conducted further refinement in a finer area. The total number of grids utilized is 3.22 million. The simulation duration is set at 300 seconds, with a time step of 0.01 seconds selected for the calculations.

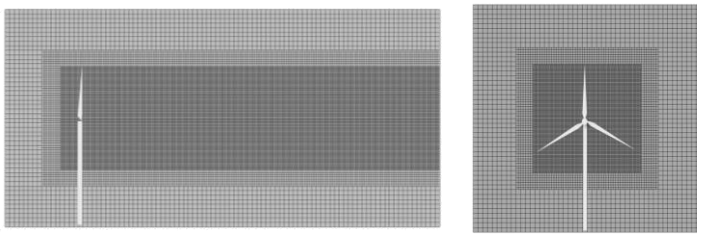

(a) xy plane (b) yz plane

Fig. 4 Computational meshes

Condition parameter setting

To investigate the impact of different forced motions on the aerodynamic performance of the wind turbine, seven sets of working conditions have been established. The specific working conditions are detailed in Table 1. The forced surge motion is set as follows:

$$x = A\sin(\frac{2\pi}{T}t) \quad (4)$$

where x is the displacement of the wind turbine in the x-direction, A is the amplitude of the forced motion, and T is the period of the forced motion.

Case0-1 and Case0-2 serve to validate the accuracy of the solution method and results. Here, blade deformation and forced motion are calculated independently and compared against reference data. In Case1 through Case5, we introduce forced surge motions with varying amplitudes and periods. Specifically, we set amplitudes of 2m, 4m, and 8m, and periods of 9s, 12s, and 15s, as guided by Wu et al. (2015).

Table 1. Specifications for simulation cases

Margins	Deformation	Motion	Period	Amplitude
Case0-1	yes	/	/	/
Case0-2	/	surge	12s	2m
Case1	yes	surge	12s	2m
Case2	yes	surge	12s	4m
Case3	yes	surge	12s	8m
Case4	yes	surge	9s	2m
Case5	yes	surge	15s	2m

VERIFICATION AND VALIDATION

Mesh convergence

To ensure the reliability and accuracy of our simulations, we conducted a series of mesh independence tests using three distinct mesh densities: coarse, medium, and fine. The coarse mesh was 1.2 times larger than the medium mesh, while the fine mesh was 0.8 times smaller. The results of the power and thrust calculations for different grids are presented in Fig. 5. We observed that the periodic nature of the results remained consistent across all mesh densities, indicating grid independence. Additionally, the amplitude differences were minimal.

Table 2 shows the number of grids and the mean values of aerodynamic power and thrust for different grids. The difference in aerodynamic power between the fine grid and the medium grid is only 1.9%, and the difference in thrust is 0.9%. This analysis confirms the convergence of the different grid calculation results. In this study, we selected the medium grid for numerical calculations to ensure both computational efficiency and accuracy.

Table 2. The grid sensitivity analysis

Mesh	Mesh quantity	Power (MW)	Thrust(N)
Coarse	1, 860, 000	5.11	649.93
Medium	3, 220, 000	5.25(2.7%)	658.66(1.4%)
Fine	5, 660, 000	5.35(1.9%)	665.24(0.9%)

Deformation

To ensure the accuracy of blade tip deformation calculations, Case0-1 was specifically designed to simulate the deformation of the turbine blades under uniform wind conditions at the rated wind speed of 11.4 meters per second. The simulation results are depicted in Fig. 6, where the deformations of flapwise, edgewise, and torsional are compared with those documented in reference. The comparison indicates that the deformations are fundamentally consistent, with no significant discrepancies noted between the simulation outcomes and the values reported in the literature.

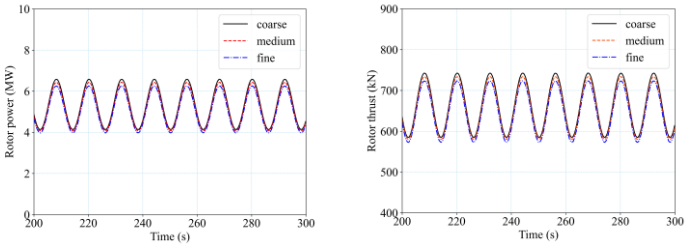

(a) Power (b) Thrust

Fig. 5 Simulation results with different grids

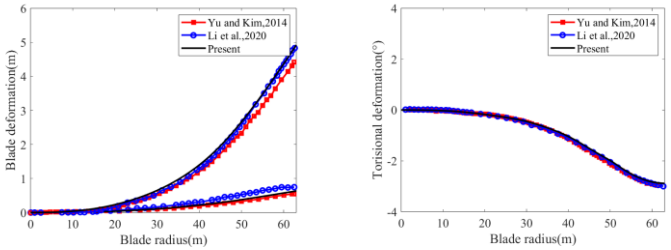

(a) Bending deformation (b) Torsional deformation

Fig. 6 Span-wise distributions of blade deflection

Forced motion

To verify the accuracy of the forced motion simulations, Case0-2 models the power and thrust of the wind turbine under uniform wind conditions at the rated wind speed of 11.4 meters per second, without accounting for blade deformation effects. Fig.7 illustrates a comparison of the power and thrust over a single cycle with the values reported in reference. The results obtained in this study are marginally higher, which may be attributed to assumptions inherent in the simulation model or particular conditions employed in the calculations. Nonetheless, these differences fall within an acceptable margin, suggesting that the simulation offers a reliable representation of the turbine's actual performance.

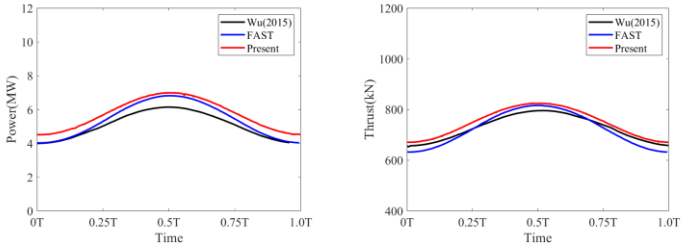

(a) Power (b) Thrust

Fig. 7 The comparison of power and thrust curves within a single cycle

RESULTS AND DISSCUSSIONS

Different amplitudes

Fig.8 illustrates the power and thrust under different amplitudes of forced motion. The period of change aligns with the period of the forced motion, and the fluctuation values increase with the amplitude of the forced motion. The relationship between the fluctuation values and the amplitude of the forced motion is nearly linear. Specifically, the average power increases by 2% and 7.2%, while the fluctuation values increase by 97.8% and 86.5%. The average thrust decreases by 0.1% and -0.1%, and the fluctuation values increase by 99.5% and 87.9%. The sharp increase in fluctuation values may be attributed to the forced motion, which induces additional velocity in the airflow around the blades, thereby altering the power and thrust of the turbine.

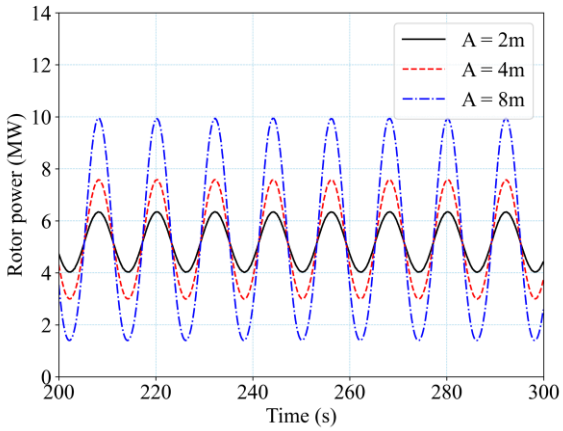

(a) Power

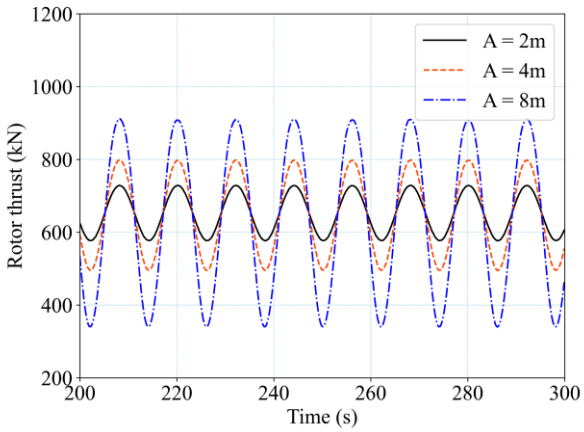

(b) Thrust

Fig. 8 Power and thrust under different amplitudes

Fig. 9 displays the attack angle under different amplitudes of forced motion. The root of the blade exhibits a significantly larger angle of attack. As the amplitude of the motion increases, the region of larger angles of attack spreads outward from the root, and the temporal variation of the attack angle becomes more pronounced. This pattern is consistent with the increase in thrust fluctuations observed in Figure x as the amplitude of the forced motion increases. When the forced motion amplitude reaches 8 meters, a large angle of attack is periodically generated from the blade root to a location at 0.5 times the

rotor radius, which significantly affects the rotor thrust.

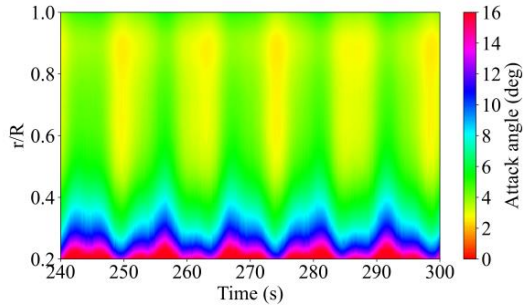

(a) A = 2m

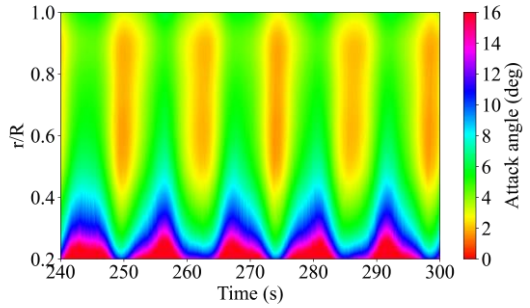

(b) A = 4m

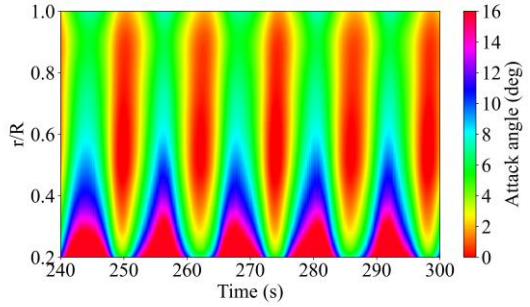

(c) A = 8m

Fig. 9 Temporal and spatial distribution of the local attack angle under different amplitudes

Fig.10 illustrates the ratio of tip deformation to wind turbine radius for different amplitudes of forced motion. As the amplitude of the forced motion increases, both the flapwise and the edgewise deformations of the blades increase. The flapwise deformation is particularly more affected by the forced motion. When the forced motion amplitude reaches 8 meters, the tip flapwise deformation exceeds 10% of the blade radius. The tip edgewise deformation, while smaller, exhibits more intense temporal variations and displays distinct second-order characteristics. These characteristics are due to the interaction between the blade's inherent natural frequency and the frequency of the forced motion.

Different periods

Fig. 11 presents the power and thrust data of a wind turbine under different periods of forced motion. Specifically, it shows that the mean power experiences a decrease of 0.7% and 0.3%, while the fluctuation values of power decrease by 23.9% and 18.6%. For the thrust, the mean value decreases by 0.9% and 3.1%, and the fluctuation values decrease by 24.1% and 18.9%. Notably, the fluctuation values are more significantly influenced by the amplitude of the motion compared to the mean values.

Fig. 12 illustrates the aerodynamic angle of attack under different periods of forced motion. As the period of the motion increases, the position of the larger angles of attack remains largely unchanged. However, the overall aerodynamic angle of attack shows an increasing trend, accompanied by more moderate fluctuations. This change in the aerodynamic angle of attack has a corresponding effect on the aerodynamic thrust, as depicted in Figure 11, where the fluctuation values of thrust decrease as the period of the motion increases.

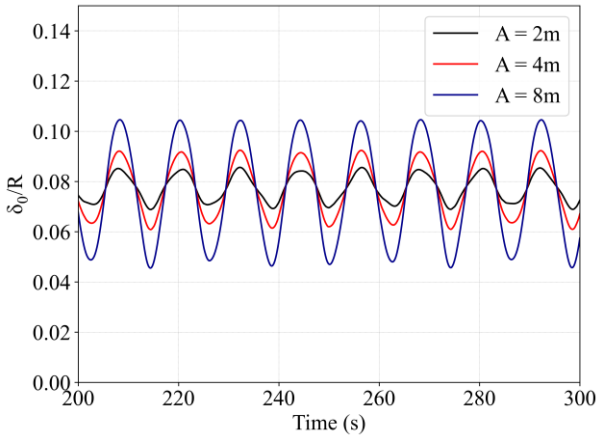

(a) Flapwise deformation

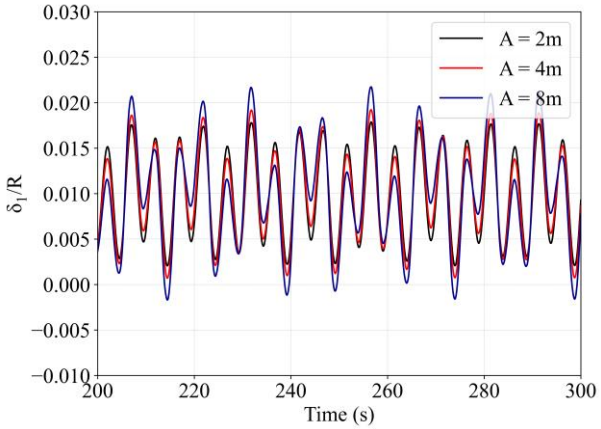

(b) Edgewise deformation

Fig. 10 Tip deformation under different amplitudes

Fig.13 shows the ratio of tip deformation to rotor radius under different periods of forced motion. As the period of the forced motion increases, the amplitudes of both the flapping and the shimmy deformations of the wind turbine blades change slightly but the differences are minimal. The mean value of the tip flapping deformation remains around 8% of the blade radius. The tip shimmy deformation is relatively small, and the variation period is completely consistent across the three working conditions, showing no significant influence from changes in the period of the forced motion. Additionally, there is no clear pattern in the changes of the maximum values.

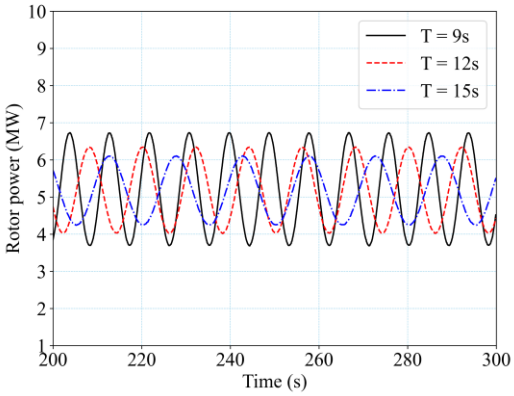

(a) Power

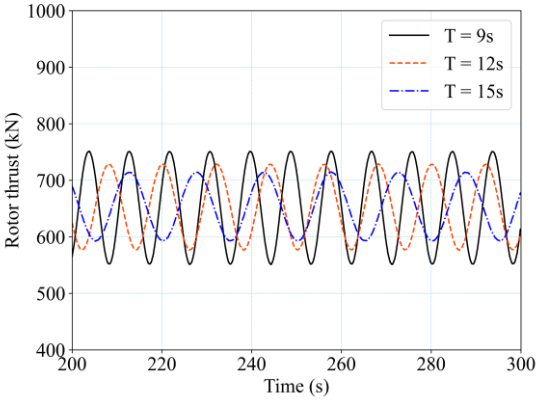

(b) Thrust

Fig. 11 Power and thrust under different periods

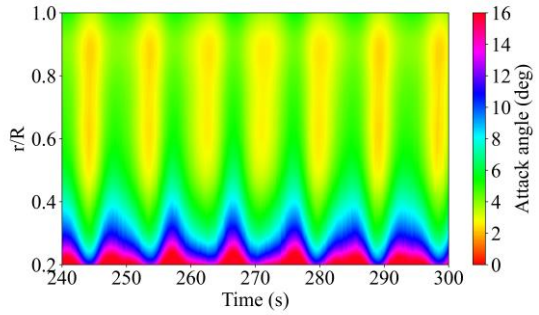

(a) T = 9s

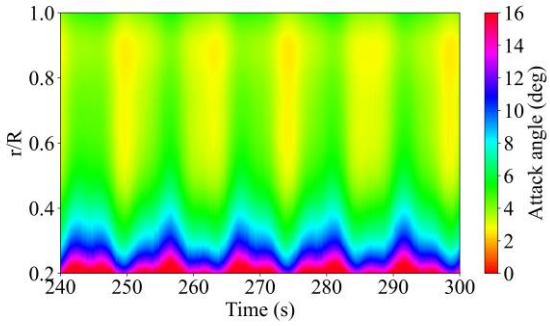

(b) T = 12s

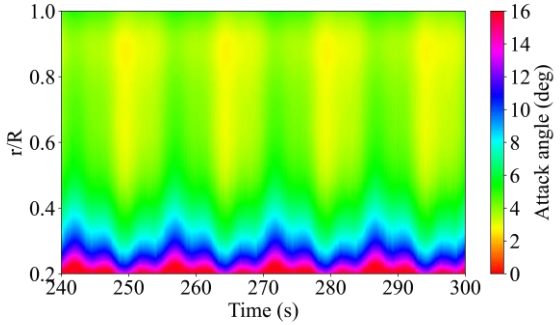

(c) T = 15s

Fig. 12 Temporal and spatial distribution of the local attack angle under different amplitudes

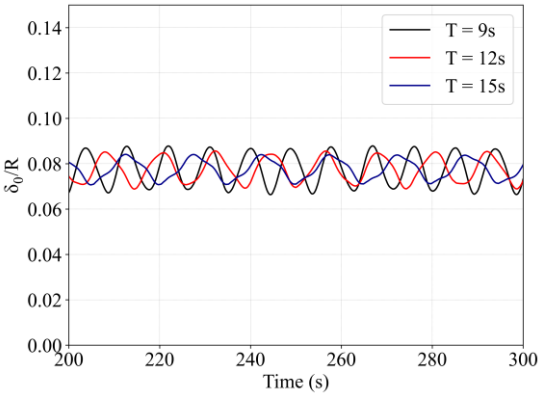

(a) Flapwise deformation

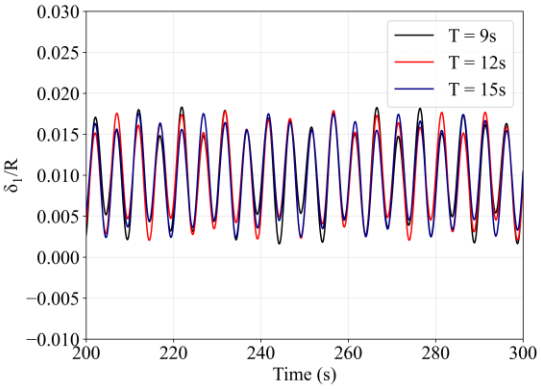

(b) Edgewise deformation

Fig. 13 Tip deformation under different periods

CONCLUSIONS

In this paper, we investigates the effects of different amplitudes and periods of forced motion on the performance and deformation of wind turbines. The results reveal several key findings.

The impact of forced motion amplitude on turbine performance shows that power and thrust fluctuations align with the forced motion period and increase nearly linearly with amplitude. Specifically, average power increases by 2% and 7.2%, while fluctuations surge by 97.8% and 86.5%. Average thrust decreases slightly by 0.1% and -0.1%, but

fluctuations rise by 99.5% and 87.9%. These sharp increases are likely due to additional velocity induced in the airflow around the blades, significantly altering turbine performance. Blade root attack angle and tip deformation also increase with amplitude, with flapwise deformation exceeding 10% of the blade radius at 8 meters amplitude. Edgewise deformation, though smaller, shows intense temporal variations and second-order characteristics due to frequency interactions. In contrast, when the period of forced motion changes, mean power and thrust decrease slightly, while fluctuation values drop more significantly by 23.9% and 18.6% for power, and 24.1% and 18.9% for thrust. The attack angle increases overall with a more moderate fluctuation, and thrust fluctuations decrease correspondingly. Blade tip deformation ratio remains largely unchanged with period, with flapwise deformation staying around 8% of the blade radius and edgewise deformation showing no significant influence or clear pattern in maximum values.

In conclusion, the amplitude of forced motion has a more pronounced impact on the power, thrust, attack angle, and deformation of wind turbines, leading to larger fluctuations and more significant changes in these parameters. In contrast, the period of forced motion has a relatively smaller effect on these aspects, with only slight changes in the mean values and more moderate fluctuations. These findings provide valuable insights for understanding the dynamic behavior of wind turbines under forced motion conditions and can guide the design and operation of wind turbines to enhance their performance and reliability.

ACKNOWLEDGEMENT

This work is supported by the National Natural Science Foundation of China (52131102), to which the authors are most grateful.

REFERENCES

Alkhabbaz, A, Hamza, H, Daabo, AM, Yang, H, Yoon, M, Koprulu, A, and Lee, YH (2024). "The aero-hydrodynamic interference impact on the NREL 5-MW floating wind turbine experiencing surge motion." *Ocean Eng*, 295, 116970.

Cai, Y, Li, X, Leng, S, Zhao, H, and Zhou, Y (2024). "Effect of combined surge and pitch motion on the aerodynamic performance of floating offshore wind turbine." *Ocean Eng*, 306, 118061.

Chen, G, Liang, X. F, and Li, X (2022). "Modelling of wake dynamics and instabilities of a floating horizontal-axis wind turbine under surge motion." *Energy*, *239*, 122110.

Cheng, P, Huang, Y, and Wan, D (2019). "A numerical model for fully coupled aero-hydrodynamic analysis of floating offshore wind turbine." *Ocean Eng*, 173, 183-196.

Meng, H, Su, H, Guo, J, Qu, T, and Lei, L (2022). "Experimental investigation on the power and thrust characteristics of a wind turbine model subjected to surge and sway motions." *Renew Energy*, 181, 1325-1337.

Fang, Y, Duan, L, Han, Z, Zhao, Y, and Yang, H (2020). "Numerical analysis of aerodynamic performance of a floating offshore wind turbine under pitch motion." *Energy*, 192, 116621.

Fang, Y, Li, G, Duan, L, Han, Z, and Zhao, Y (2021). "Effect of surge motion on rotor aerodynamics and wake characteristics of a floating horizontal-axis wind turbine." *Energy*, 218, 119519.

Feng, X, Lin, Y, Zhang, G, Li, D, Liu, H, and Wang, B (2021). "Influence of combined motion of pitch and surge with phase difference on aerodynamic performance of floating offshore wind turbine." *J Mar Sci Eng*, 9(7), 699.

Fontanella, A, Zasso, A, and Belloli, M (2022). "Wind tunnel investigation of the wake-flow response for a floating turbine subjected to surge motion." *In Journal of Physics: Conference Series*, IOP Publishing, 2265(4): 042023.

Jonkman, J (2009). "Definition of a 5-MW Reference Wind Turbine for Offshore System Development." National Renewable Energy Laboratory.

Li, Z, Wen, B, Dong, X, Peng, Z, Qu, Y, and Zhang, W (2020). "Aerodynamic and aeroelastic characteristics of flexible wind turbine blades under periodic unsteady inflows." *J Wind Eng Ind Aerodyn*, 197, 104057.

Liu, Y, Xiao, Q, Incecik, A, and Peyrard, C (2019). "Aeroelastic analysis of a floating offshore wind turbine in platform‐induced surge motion using a fully coupled CFD‐MBD method." *Wind Energy*, 22(1), 1-20.

Schulz, CW, Netzband, S, Özinan, U, Cheng, PW, and Abdel-Maksoud, M (2023). "Wind turbine rotors in surge motion: New insights into unsteady aerodynamics of FOWT from experiments and simulations." *Wind Energy Sci Discuss*, 2023, 1-47.

Sivalingam, K, Martin, S, and Singapore Wala, AA (2018). "Numerical validation of floating offshore wind turbine scaled rotors for surge motion." *Energies*, 11(10), 2578.

Tran, TT, Kim, DH (2016). "A CFD study into the influence of unsteady aerodynamic interference on wind turbine surge motion." *Renew Energy*, 90, 204-228.

Wang, K, Zhao, M, Chen, S, and Zha, R (2024). "Aerodynamic performance analysis of a floating wind turbine with coupled blade rotation and surge motion." *Eng Appl Comput Fluid Mech*, 18(1), 2301524.

Wen, B, Tian, X, Dong, X, Peng, Z, and Zhang, W (2017). "Influences of surge motion on the power and thrust characteristics of an offshore floating wind turbine." *Energy*, 141, 2054-2068.

Wu, J, Ding, JH, He, YP, and Zhao, YS (2015). "Study on unsteady aerodynamic performance of floating offshore wind turbine by CFD method." *Int J Offshore and Polar Eng*, ISOPE, 2015, 554‐560.

Yu, DO, Kwon, OJ (2014). "Predicting wind turbine blade loads and aeroelastic response using a coupled CFD–CSD method." *Renew Energy*, 70, 184-196.